


RESEARCH

Open Access



Bone char modification by iron to improve its capacity for adsorbing fluoride from an aqueous solution

Damarys Haydee Carrales-Alvarado¹, Brenda Azharel Jiménez-López¹, Roberto Leyva-Ramos^{1*} , Nahum Andrés Medellín-Castillo², Esmeralda Mendoza-Mendoza^{1,3}, Carolina Vázquez-Mendoza¹ and Diana Elizabeth Villela-Martínez¹

Abstract

High fluoride concentrations in groundwater have attracted great concern worldwide because many people are afflicted by fluorosis due to water consumption. In this work, the fluoride adsorption from water onto bone char (BC) modified with iron sulfate (BCM) was studied as an option for eliminating fluoride from drinking water. The experimental data for the adsorption equilibrium of fluoride on BCs were procured in a batch adsorber. The synthesis conditions of BCs were optimized for improving the adsorption capacity of BCs, and the optimal BCM was designated as BCM2. The BCs were characterized by different analytical techniques, the BCs surface exhibited an irregular morphology and the chemical nature was basic, and the BCs were mesoporous materials. The Langmuir isotherm satisfactorily interpreted the experimental data of the fluoride adsorption isotherms on BCs. The basic sites of BC and BCs were quantified and identified in this work. The main adsorption mechanism of fluoride on the BCs was the electrostatic attraction between the fluoride and the basic sites of BCs, and the adsorption capacities of BC and BCs towards fluoride increased almost linearly with the concentration of basic sites so that the enhancement of the adsorption capacity of BCs was attributed to the increase of basic sites during the modification. Furthermore, the BCM2 adsorption capacity was lessened by incrementing the pH from 5 to 9, and this behavior was ascribed to the reduction of the electrostatic attraction interactions between the BCM2 surface basic sites and fluoride in the solution. The adsorption process was endothermic because the adsorption capacities of BC and BCM2 toward fluoride were raised by incrementing the solution temperature from 15 to 35 °C. The BCM2 presented a high capacity for adsorbing fluoride of 14.4 mg g⁻¹ at 25 °C and a pH of 5.

Keywords Adsorption, Bone char, Fluoride, Iron nanoparticles, Drinking water

1 Introduction

Population growth has brought diverse environmental impacts, and water is one of the most affected sources concerning the loss of accessibility and contamination of surface and groundwater [1]. Water shortage has already shown damaging effects worldwide. Recently, the World Health Organization (WHO) and the United Nations Children's Fund reported that more than 2,000 million have access to a limited water supply, and 771 million

*Correspondence:

Roberto Leyva-Ramos
rlr@uaslp.mx

¹ Center for Research and Graduate Studies, School of Chemistry, Autonomous University of San Luis Potosí, 78260 San Luis Potosí, Mexico

² School of Engineering, Autonomous University of San Luis Potosí, 78260 San Luis Potosí, Mexico

³ Catedras Program, National Council for Research and Technology, 03940 Mexico City, Mexico



© The Author(s) 2023. **Open Access** This article is licensed under a Creative Commons Attribution 4.0 International License, which permits use, sharing, adaptation, distribution and reproduction in any medium or format, as long as you give appropriate credit to the original author(s) and the source, provide a link to the Creative Commons licence, and indicate if changes were made. The images or other third party material in this article are included in the article's Creative Commons licence, unless indicated otherwise in a credit line to the material. If material is not included in the article's Creative Commons licence and your intended use is not permitted by statutory regulation or exceeds the permitted use, you will need to obtain permission directly from the copyright holder. To view a copy of this licence, visit <http://creativecommons.org/licenses/by/4.0/>.

people do not have sufficient and secure water resources [2].

WHO has classified fluoride, arsenic and nitrate as major water contaminants for human consumption because these pollutants can cause large-scale health problems [3]. More than 70 million people in 25 countries are afflicted with fluorosis [4]. Fluoride contamination occurs mainly from geological sources or from industries that use raw materials that contain fluoride. An ample diversity of minerals present in the soil contain fluorine in their structure, for example, fluorite, apatite, cryolite, mica, sellaite, phlogopite, topaz and others [5, 6]. The most important sources of anthropogenic contamination are industrial, mining and agricultural activities [7].

There are different processes for separating fluoride from aqueous solutions [8]; however, adsorption is the most cost-effective method for water defluorination [9]. Diverse adsorbents have been tested for eliminating fluoride present in drinking water; among them are activated alumina [10], ion exchange resins [11], layered double hydroxide [12] and cellulosic materials [13]. Additionally, traditional adsorbents have been modified to increase their capacity for adsorbing fluoride; for example, activated alumina coated with manganese dioxide [14], rice husk coated with aluminum hydroxide [15], aluminum-impregnated activated carbon [16] and polymeric resins impregnated with trivalent metals like Ce(III), La(III) and Y(III) [17, 18].

Bone char (BC) is manufactured by charring animal bones, primarily cattle, and using an oven operated from 500 to 700 °C for 4–6 h in an inert atmosphere [19, 20]. For some time, BC has been considered an appropriate adsorbent for eliminating fluoride from water [19, 21], mainly due to its low cost [22]. Leyva-Ramos et al. [20] reported that the adsorption capacity of BC towards fluoride could be ascribed essentially to the hydroxyapatite present in BC; hence, the chemical alteration of the BC surface can promote the BC adsorption capacity [22].

In some works, the BC surface was altered to upgrade its adsorption capacity toward fluoride, and the modification of BC has been carried out by metal doping or acid

treatment. BC was modified by washing with 0.1 M HCl and then doping with Al(III), Ca(II), Mg(II), or Fe(III) in HCl 1.5% w/w solutions and the adsorption capacities of the BCMs ranged from 1.6 to 6.8 mg g⁻¹ [23]. Alkurdi et al. [6] reviewed the modification of BC and noted that the capacity of BC had been successfully increased by impregnating the BC with Ce(III), Ce(IV) and Al(III), and Ce(IV)-doped BC presented a high capacity for adsorbing fluoride [24]. Medellin-Castillo et al. [22] modified BC by thermal treatment and acid treatment using 1.0 M HNO₃ solutions and found that the chemical modification improved the BC adsorption capacity towards fluoride but not the thermal treatment. However, the dependence of the adsorption capacity of BMCs on the basic sites concentration has not been analyzed in previous works.

This work aimed to upgrade the BC adsorption capacity for fluoride by chemical modification of the BC surface using iron sulfate solutions at different conditions to attain the maximum adsorption capacity of BC doped with iron. Besides, the adsorption mechanism of fluoride on BCM and the role of basic sites on the adsorption capacity were elucidated in this work.

2 Experimental methods

2.1 Bone char

A commercial BC was utilized in this study and was fixed by calcining cattle bones by the APELSA company, Mexico. The reagent grade chemicals used were NaF, FeSO₄·7H₂O and NH₄Fe(SO₄)₂·12H₂O and were purchased from Sigma–Aldrich, Mexico.

2.2 Procedure for modifying BC

Predetermined amounts (millimoles) of FeSO₄·7H₂O and NH₄Fe(SO₄)₂·12H₂O were added to a volumetric flask (150 mL) and were dissolved using a specific volume (6–24 mL) of concentrated H₂SO₄ solution, V_{Acid} (See Table 1). Subsequently, the volumetric flask was filled with distilled water up to the mark, and the suspension was poured into an Erlenmeyer flask containing a certain mass of BC (M_{BC}). As listed in Table 1, the modifying conditions were varied by increasing the millimoles of

Table 1 Experimental conditions for modifying the BC with iron sulfate

Designation of BCM	M _{BC} (g)	FeSO ₄ ·7H ₂ O (mmol)	NH ₄ Fe(SO ₄) ₂ ·12H ₂ O (mmol)	V _{Acid} (mL)	Ratio V _{Acid} /M _{BC} (mL g ⁻¹)
BCM1	20	0.018	0.021	6	3/10
BCM2	20	0.036	0.042	12	6/10
BCM3	10	0.036	0.042	12	12/10
BCM4	10	0.072	0.084	24	24/10

iron salts and decreasing the M_{BC} because the adsorption sites of BCM depend on the iron loading. Then, 140 mL of 1.5 M NaOH solution was poured dropwise into the Erlenmeyer mixture (the dropping lasted for more than 60 min) and mixed continuously at room temperature. Moreover, the suspension was vigorously stirred for 17 h, then 100 mL of 3 M NaOH solution was added dropwise (the addition took more than 30 min), followed by vigorous stirring for 4 h. The BCMs were rinsed employing distilled water three times, filtrated and dried at 50 °C during 15 h, as described by Asfaram et al. [25]. The final pH of the rinsing solution ranged between 7 and 8. As shown in Table 1, the BCM was designated based on the modification conditions, such as the ratio of V_{Acid}/M_{BC} and that of the millimoles of iron salts to M_{BC} .

2.3 Physicochemical and textural properties of BC and BCMs

The volumetric titration technique recommended by Boehm [26] was utilized to appraise the concentrations of basic and acidic sites, and the acid–base titrating technique outlined by Flores-Cano et al. [27] was employed to assess the point of zero charge (pH_{PZC}) and surface charge distribution. Both acid–base titration methods were thoroughly described by Medellin-Castillo et al. [21]. The average pore diameter (D_p), pore volume (V_p), and surface area (S_{BET}) were assessed employing the Nitrogen adsorption–desorption isotherm appraised in an N_2 physisorption analyzer (Micromeritics, ASAP 2020) at 77 K. Prior to the measurement the samples were outgassed overnight at 110 °C under high vacuum (10^{-4} Pa). The Brunauer–Emmett–Teller (BET) procedure [28] was implemented to compute the S_{BET} .

2.4 Characterization of BC and BCMs

The BC and BCMs surface morphology was observed by scanning electron microscope (SEM) (Philips, model XL-30) at an accelerating voltage of 10 kV. Furthermore, the morphology of BCM2 was investigated by employing a scanning transmission electron microscope (STEM) (JEOL, JEM 1400) operated at an accelerating voltage of 120 kV. The crystalline phases in the materials were identified by performing the X-ray diffraction (XRD) analysis utilizing a diffractometer (Bruker, D8 Advance). XRD patterns were recorded from 4 to 90° (2θ) at a scanning rate of $1.8^\circ \text{ min}^{-1}$ and obtained under operating conditions of Cu-K α radiation ($\lambda = 0.15406 \text{ nm}$), 35 mA and 40 kV.

2.5 Analysis of fluoride in water solution

The fluoride quantification in a water sample was performed by an electrometric technique utilizing a potentiometer (Orion, model 420 A+) and a fluoride

selective electrode (Orion, model 249,030-A01). The fluoride concentration was appraised utilizing a calibration curve, fluoride concentration (mg L^{-1}) vs. potential (mV), fixed using eight standard fluoride solutions with concentrations varying between 0.3 and 50 mg L^{-1} . These standard solutions were prepared by diluting a stock fluoride solution of 100 mg L^{-1} . More details of the analytical method were outlined earlier by Leyva-Ramos et al. [16] and Medellin-Castillo et al. [21].

2.6 Methodology for procuring the adsorption capacity data

A standard fluoride solution of 100 mg L^{-1} was made by supplementing NaF (0.221 g) into a volumetric flask (1000 mL) and filling it with deionized water up to the line marked. Besides, a solution of constant ionic strength and particular pH was made by combining suitable portions of 0.01 N HNO_3 and NaOH solutions. At a specific pH, fluoride solutions having initial concentrations between 1 and 40 mg L^{-1} were made by pouring an aliquot of the standard fluoride solution into a volumetric flask (50 mL) and filling up to the line marked with the solution of constant ionic strength and specific pH. A sample of 10 mL was taken to verify the initial concentration afterward. The remaining fluoride solution (40 mL) was poured into a plastic vial (batch adsorber) containing 0.1 g of the adsorbent.

The adsorber was set inside a thermostatic water bath to maintain the adsorber solution temperature constant. The solution in the adsorber was mechanically mixed by setting the adsorber on top of an orbital shaker, TS-100, for 25 min four times daily. The solution pH in the adsorber was regularly appraised employing a pH meter and was held constant by supplementing a few drops of 0.01 N NaOH or HNO_3 solutions, as necessary. In prior studies, it was found that 7 d were sufficient to approach equilibrium; therefore, the fluoride solution and the adsorbent were contacted for 8 d to ensure that equilibrium was ultimately attained. Afterward, a solution sample was analyzed to quantify the equilibrium fluoride concentration, and the uptake of fluoride adsorbed was calculated through a fluoride mass balance, described by the succeeding mathematical relationship:

$$q = \frac{V(C_0 - C)}{m} \quad (1)$$

where C_0 is the fluoride concentration at the beginning, mg L^{-1} ; C is the equilibrium fluoride concentration, mg L^{-1} ; m is the adsorbent mass, g; q is the amount of fluoride adsorbed on the material, mg g^{-1} ; and V is the adsorber solution volume, L.

2.7 Fitting isotherm models to the adsorption data of fluoride

The Langmuir, Freundlich and Radke-Prausnitz isotherms have been extensively employed to interpret the adsorption equilibrium in aqueous-solid adsorbent systems. The subsequent equations can mathematically express these isotherm models:

$$q = \frac{q_m KC}{1 + KC} \tag{2}$$

$$q = kC^{1/n} \tag{3}$$

$$q = \frac{aC}{1 + bC^{1-\beta_{RP}}} \tag{4}$$

where a ($L\ g^{-1}$), b ($L^{1-\beta_{RP}}\ mg^{\beta_{RP}-1}$) and β_{RP} are the constants for the Radke-Prausnitz isotherm; K ($L\ mg^{-1}$) and q_m ($mg\ g^{-1}$) are the constants for the Langmuir isotherm; n and k ($L^{1/n}\ mg^{1-1/n}\ g^{-1}$) are the constants for the Freundlich isotherm.

The estimation of the constants was carried out by fitting the isotherm equations to the experimental data utilizing a least-squares nonlinear regression procedure based upon the optimization methods of Rosenbrock and quasi-Newton. Besides, the average absolute percentage deviation was assessed by the succeeding mathematical expression:

$$\%D = \frac{1}{N} \sum_{i=1}^N \left| \frac{q_{exp} - q_{pred}}{q_{exp}} \right| \times 100\% \tag{5}$$

where N is the number of experimental data; q_{pred} is the fluoride uptake appraised with the adsorption isotherm equation, $mg\ g^{-1}$; q_{exp} is the experimental fluoride uptake, $mg\ g^{-1}$. The adsorption isotherm having the smallest %D was assumed to be the isotherm equation yielding the best fit.

3 Results and discussion

3.1 X-Ray diffraction assay

Figure 1 depicts XRD patterns of BC, BCM2 and BCM2 saturated with fluoride (F/BCM2). The hydroxyapatite $[Ca_{10}(PO_4)_6(OH)_2]$ crystalline phase (JCPDS 86-1201) was identified in BC and BCM2. It is very well known that hydroxyapatite was the main constituent of BC [29]. After adsorbing fluoride, the hydroxyapatite crystal structure was confirmed in F/BCM2. No additional diffraction peaks were observed in the XRD pattern of F/BCM2, revealing that the fluoride adsorption did not modify the hydroxyapatite crystal structure.

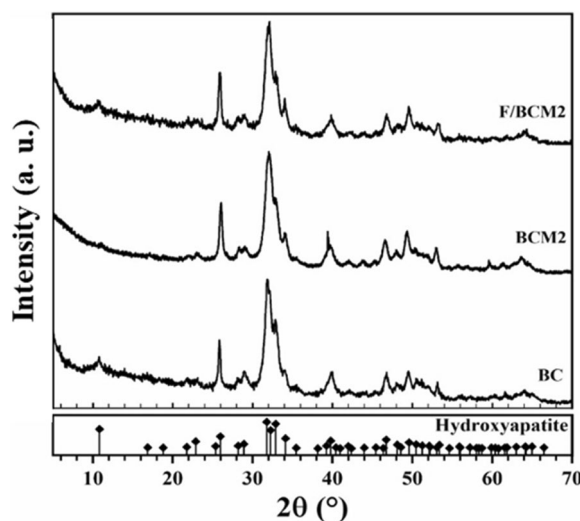


Fig. 1 XRD patterns of BC, BCM2, and F/BCM2. The standard of hydroxyapatite is at the bottom

Table 2 Textural and physicochemical properties of BC and modified BCs

Adsorbent	S_{BET} ($m^2\ g^{-1}$)	V_p^1 ($cm^3\ g^{-1}$)	D_p^2 (nm)	Concentration of sites ($meq\ g^{-1}$)	
				Acidic	Basic
BC	75	0.23	12.3	0.25	2.11
BCM1	11	0.12	39.7	N.D. ³	2.69
BCM2	48	0.16	13.3	1.58	5.40
BCM3	23	0.10	16.6	0.37	3.75
BCM4	7	0.02	12.7	N.D. ³	1.99

¹ Total pore volume determined at $P/P^0 \approx 0.99$

² Average pore diameter calculated by the following equation $D_p = 4V_p/S_{BET}$

³ N.D. No Detected

3.2 Textural characteristics of BC and BCMs

The textural characteristics of the BC and BCMs are registered in Table 2. The V_p and S_{BET} of BC were slightly less than those reported in an earlier study [22], whereas the D_p was slightly higher. The values of D_p ranged from 12 to 40 nm, substantiating that the BC and BCMs are mesoporous materials. As noticed in Table 2, the S_{BET} of BC and BCMs decreased in the following order $BC > BCM2 > BCM3 > BCM1 > BCM4$ and were dependent on the ratio of V_{Acid}/M_{BC} . The S_{BET} and V_p of BCM2 were less affected than those of the other BCMs. In general, S_{BET} and V_p of BC diminished around 11 times when the ratio of V_{Acid}/M_{BC} was raised eightfold. However, as described later, the adsorption capacity of BCMs did not decrease in the same order as the surface area. Similar

results were reported when BC was modified by hydrothermal treatment in an HNO_3 solution [22]. In the modification, the original porous structure of BC was altered due to the BC dissolution by H_2SO_4 and the blocking out of the pores caused by impregnating BC using iron salts.

The N_2 adsorption–desorption isotherms of all the materials at 77 K are displayed in Fig. 2. Except for BCM4, the isotherm shapes were Type IV(a) [30], corresponding to mainly mesoporous materials and exhibited hysteresis loops, confirming the presence of mesoporosity in these materials. The hysteresis loop is classified as Type H3 and is typical of aggregations of platy particles [30, 31] associated with the hydroxyapatite sheets present in BC. The mesopores originated from the spaces between the hydroxyapatite sheets. The shape of the BCM4 isotherm is Type III and does not present a hysteresis loop. Therefore, this material has a very low mesoporosity and surface area.

3.3 Characterization by SEM and TEM analysis

The characterization of all the BCMs particles showed that the morphology of all the BCMs particles was very similar. The characterization of BCM2 was only argued in this section because the BCM2 presented the highest adsorption capacity towards F. The SEM images of BCM2 depicted in Fig. 3a display irregular flake-like particles with heterogeneous sizes, and the particles are staked and agglomerated due to small dimensions. Figure 3b shows that the BCM2 surface is unsmoothed at higher magnifications. The TEM micrographs of BCM2 (Fig. 3c and d) exhibit rice and needle crystal shapes [32] which are observed in the areas selected by circle and square dashed lines, respectively. Rice shape particles have a small diameter and length, whereas needle shape

particles appear with small diameters, longer lengths, and uniform morphology. It is important to point out that Mansour et al. [32] reported that the hydroxyapatite particle shape is quite sensible to the solution pH. Typically, rice morphology is associated with isotropic crystal growth at basic pH, while needle particles are obtained at $\text{pH}=7$. Hence, the BCM2 is constituted of rice and needle-like hydroxyapatite crystals because the final pH of the rinsing solution was between 7 and 8.

Figure 4a shows a dark-field TEM image of BCM2. Chemical mapping micrographs of BCM2 were acquired using STEM-EDS techniques and are depicted in Fig. 4b to d. As seen in these figures, Ca, P and O spatial distribution are associated with the hydroxyapatite phase.

The spectrum of the energy dispersive spectroscopy (EDS) microanalysis of BCM2 is depicted in Fig. 5, corroborating the presence of C, Ca, Fe, Na, O, P and S. The intensity of the C peak is high because the carbon in BCM2 comes from the calcite carbonates and carbon present in BC and carbon used for coating the BCM2 before the TEM analysis. The intensity of the O peak is high because it is associated with the presence of carbonates, phosphates and sulfates in BCM2. The presence of Fe in the BMC2 is confirmed and is due to the BC modification.

3.4 Chemical characteristics of BCM surface

The surface of BC comprises both acidic and basic sites, which are responsible for the surface charge of BC in an aqueous solution [33]. Table 2 presents the acidic and basic sites concentrations in BC and BCMs. Usually, the concentration of acidic sites in BC is lower than that of basic sites [21]. The BCMs and BC surface character is basic because the concentrations of basic sites in all materials were consistently larger than those of the acidic sites. For example, the basic sites concentration of BCM2 is 3.4-fold higher than that of the acidic sites. As expected, the modification conditions affect the basic and acidic sites.

The surface charge distribution for BCM2 and BC is displayed in Fig. 6, and the surface charge relies upon the amount and character of the functional groups on the surface and the solution pH. As shown in this figure, the pH_{PZC} of BCM2 and BC are 10.3 and 8.9, respectively, substantiating the basic character of BCM2 and BC and that the acidic sites concentration is less than that of the basic ones. The basic nature of the surface of BCM2 favors the adsorption of anions because the surface is positively charged, attracting the anions from the solution. The adsorbent surface charge distribution can explain the influence of the electrostatic interactions on the adsorption capacity.

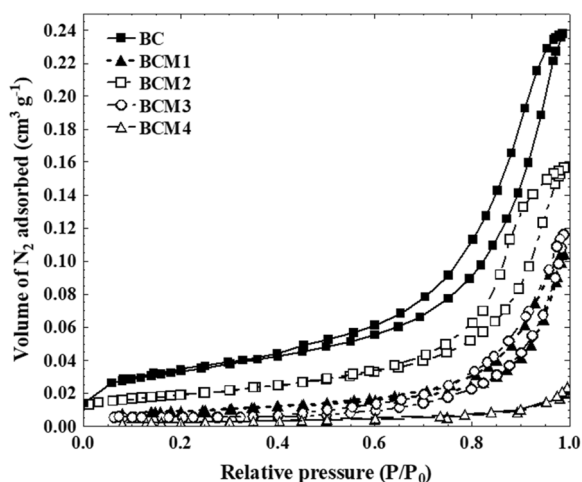


Fig. 2 Adsorption–desorption isotherms of N_2 on BC and BCMs at $T=77\text{ K}$

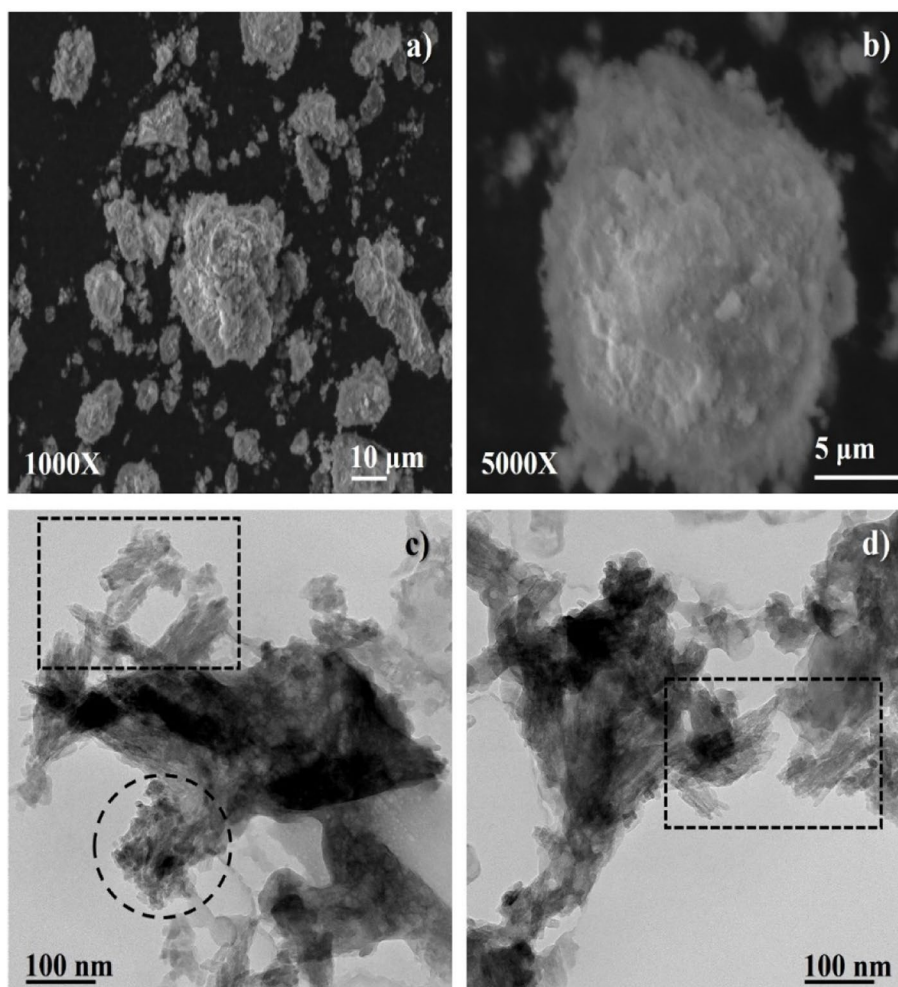
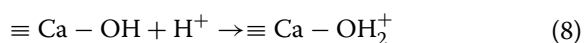
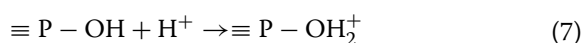
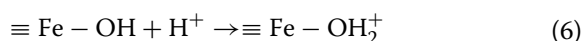


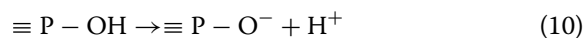
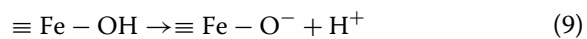
Fig. 3 SEM (a and b) and TEM (c and d) micrographs of BCM2

The functional groups of BC and BCM2 are the hydroxyls, $\equiv\text{Ca-OH}$, and the phosphates, $\equiv\text{P-OH}$, which belong to hydroxyapatite [34]. Likewise, the Fe hydroxyls, $\equiv\text{Fe-OH}$, are additionally present in BCM2 and formed during the modification [35]. The positively charged surface of the BC and BCM2 can be attributed to the subsequent protonation reactions [34, 35]:



where \equiv represents the BC or BCM2 surface. The above functional groups are the basic sites of BC and BCM2. Nevertheless, the subsequent deprotonation

reactions yield the negatively charged surface of the BC and BCM2 [34, 35]:



These three functional groups are the acidic sites of BC and BCM2. Moreover, the deprotonation and protonation reactions happened at $\text{pH} > \text{pH}_{\text{PZC}}$ and $\text{pH} < \text{pH}_{\text{PZC}}$, respectively.

Comparing the charge distribution of BCM2 with that of BC (See Fig. 6), it can be noticed that the modification of BC heightened the maximum surface charge considerably from 800 to 3000 C g⁻¹, and the pH_{PZC} of BCM2 is more basic than the pH_{PZC} of BC. These

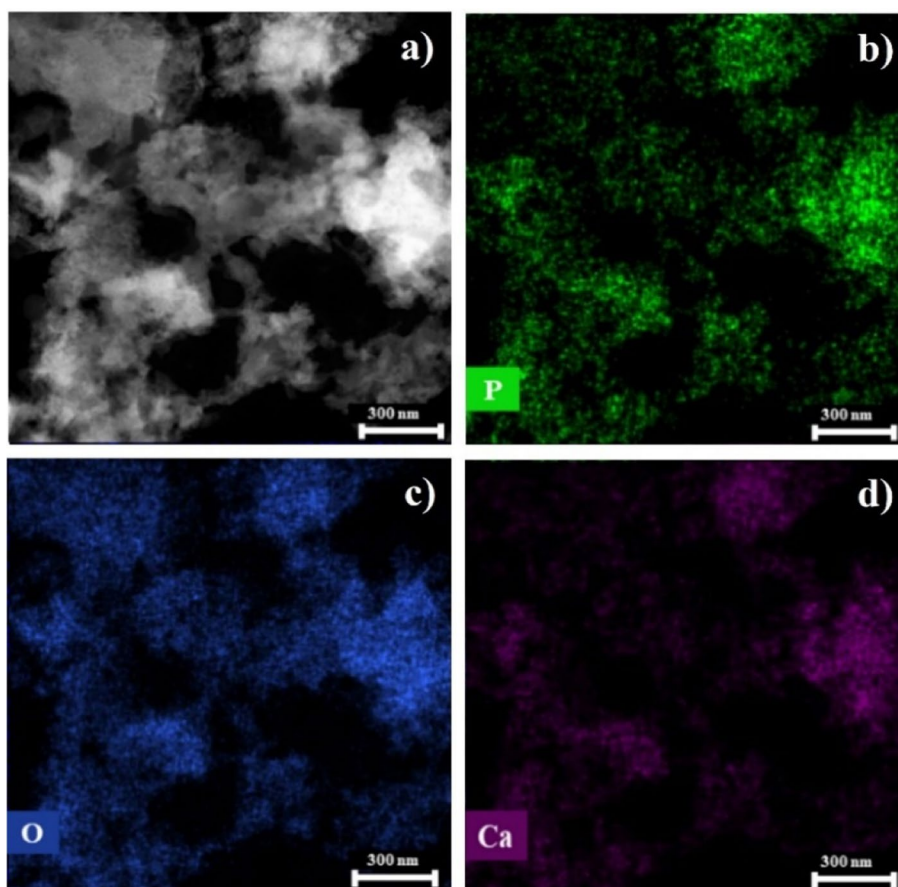


Fig. 4 Dark-field TEM image (a) and STEM-EDS analysis (b-d) of BCM2

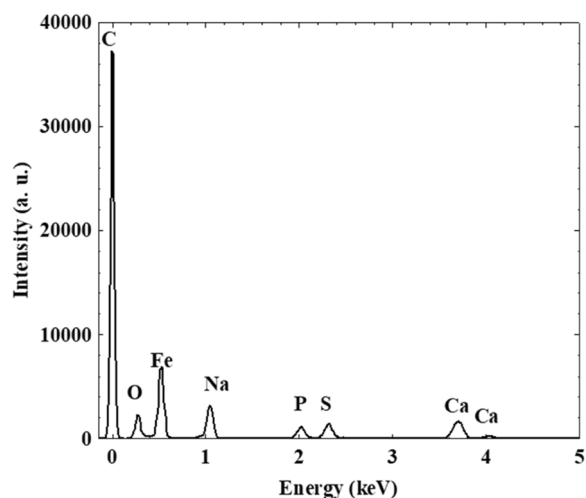


Fig. 5 EDS microanalysis of BCM2

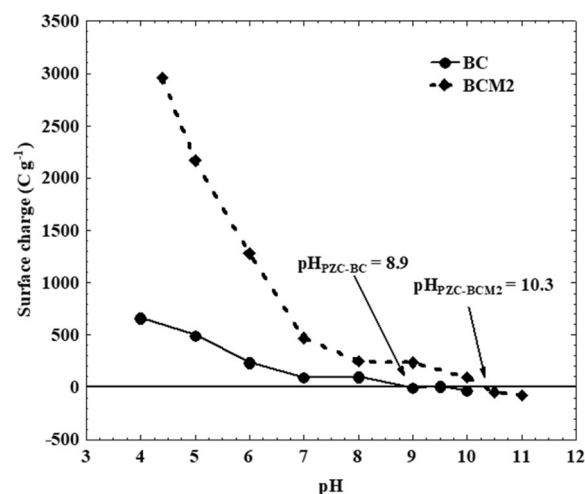


Fig. 6 Surface charge distribution of BC and BCM2

results can be explicated by remembering that the concentration of basic sites of BCM2 was raised 3.4 times after the modification.

3.5 Adsorption isotherms of fluoride on BC and BCMs

The experimental data for fluoride adsorption onto BC and BCMs were interpreted employing the Radke-Prausnitz,

Table 3 Parameters of the Freundlich, Langmuir and Radke-Prausnitz isotherms for the fluoride adsorption on BC and BCMs from aqueous solution at different pH and temperature

Material	pH	T (°C)	Freundlich			Langmuir			Radke-Prausnitz				
			k ($L^{1/n} mg^{1-1/n} g^{-1}$)	n	%D	K ($L mg^{-1}$)	q_m ($mg g^{-1}$)	%D	a ($L g^{-1}$)	b ($L^{1-\beta_{RP}} mg^{\beta_{RP}-1}$)	β_{RP}	%D	
BC	7	25	1.27	2.42	11	0.46	4.07	2.6	1.52	0.24	-0.17	3.0	
BCM1			3.28	3.56	16	1.37	7.07	9.2	9.58	1.35	0.00	9.2	
BCM3			2.58	2.59	17	0.40	8.36	12	7.81	1.91	0.76	12	
BCM4			0.75	2.27	12	0.10	4.36	28	2.88	3.12	0.39	12	
BCM2	5	25	4.39	2.18	13	0.49	14.4	7.6	9.45	0.97	0.16	4.4	
		7	15	2.98	3.00	10	0.63	7.94	23	13.8	3.17	0.20	13
		25	4.17	2.90	27	0.95	10.2	17	8.91	0.75	-0.06	21	
		35	4.81	2.99	16	1.14	11.2	9.7	16.7	1.87	0.09	4.8	
	9	25	0.73	2.21	14	0.13	4.05	7.8	0.61	0.21	0.09	9.5	

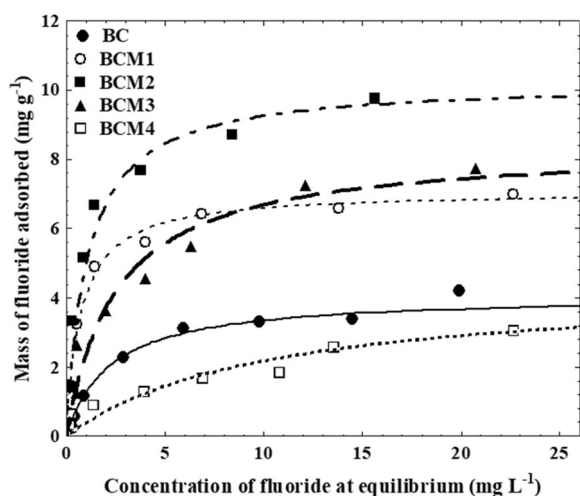


Fig. 7 Adsorption isotherms of fluoride from aqueous solution onto BC, BCM1, BCM2, BCM3 and BCM4, at $T = 25\text{ }^\circ\text{C}$ and $\text{pH} = 7$. The lines represent the Langmuir isotherm prediction

Langmuir and Freundlich isotherms, described in Sect. 2.7. Table 3 lists the parameters of these three isotherms. The outcomes show that the Langmuir model is the isotherm that best fitted the experimental data because it presented the lowest percentage of deviation in 5 out of 9 different experimental conditions tested in this work. This result was expected because the experimental data exhibited the Langmuir typical behavior of increasing the mass of fluoride adsorbed as the fluoride concentration is raised and then leveling off at higher concentrations.

3.6 Dependence of the adsorption capacity on the modification conditions

The capacities of BC and BCMs for adsorbing fluoride are compared in Fig. 7, and the

decreasing order of adsorption capacities is as follows: $\text{BCM2} > \text{BCM3} > \text{BCM1} > \text{BC} > \text{BCM4}$. For an equilibrium concentration of 15 mg L^{-1} , the mass adsorbed of fluoride on BC and BCMs was computed from the Langmuir isotherm and was named Q_{15} . This fluoride concentration at equilibrium was selected because this is the maximum fluoride concentration where there were experimental values for the mass adsorbed on BC and all BCMs. The values of Q_{15} were estimated from the Langmuir isotherm to be 9.5, 7.2, 6.7, 3.6 and 2.6 mg g^{-1} for BCM2, BCM3, BCM1, BC, and BCM4, respectively. The above outcome demonstrates that the adsorption capacity of BCM depends on the modification conditions, and BCM2 had the maximum adsorption capacity. The BCM4 adsorption capacity was even less than that of BC, implying that the modification decreased the adsorption capacity. The synthesis conditions of BCM2 are optimal since the maximum adsorption capacity was achieved, finding that the adsorption capacity of BCM2 is around 3.6 times higher than that of BC.

The enhancement and decrease of the capacities for adsorbing fluoride are associated with the concentration of basic sites because the fluoride anions were adsorbed on the basic sites. The dependence of Q_{15} upon the concentration of basic sites is illustrated in Fig. 8. As expected, the adsorption capacity increased almost linearly by raising the concentration of basic sites, corroborating its importance on the adsorption capacity.

3.7 Dependence of the BCM2 adsorption capacity towards fluoride on solution pH

At $T = 25\text{ }^\circ\text{C}$, the isotherms for fluoride adsorption on BCM2 were assessed at pH 5, 7 and 9 to study the effect of pH, and are shown in Fig. 9. No adsorption equilibrium experiment was conducted at $\text{pH} = 3$ because the

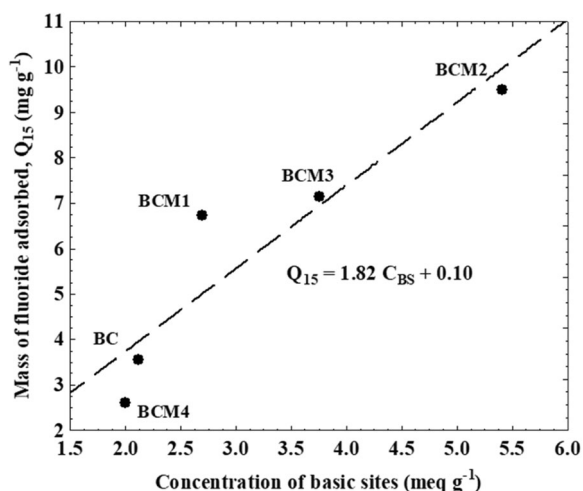


Fig. 8 Effect of the concentrations of basic sites (C_{BS}) upon the capacity of BC and BCMs for adsorbing fluoride from aqueous solution at $T = 25\text{ }^\circ\text{C}$ and $\text{pH} = 7$

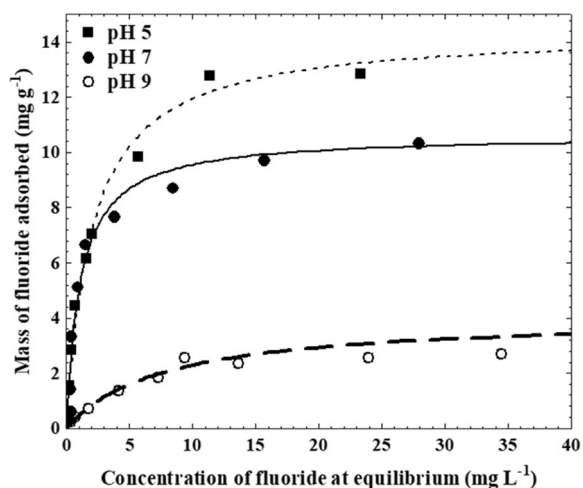


Fig. 9 Effect of solution pH upon the adsorption capacity of BCM2 towards fluoride from aqueous solution at $T = 25\text{ }^\circ\text{C}$. The lines represent the Langmuir isotherm prediction

hydroxyapatite in BC could be dissolved in this acidic condition, as reported by Medellin-Castillo et al. [34]).

Figure 9 illustrates that the BCM2 adsorption capacity diminished significantly by incrementing the pH from 5 to 9, an alike tendency was also noted in the fluoride adsorption on BC and arsenic (V) on BC modified by supporting iron nanoparticles on BC [21, 36].

For a fluoride concentration of 20 mg L^{-1} , the capacities for adsorbing fluoride were $2.1, 9.7$ and 13 mg g^{-1} at pH 9, 7 and 5, respectively. In the pH range of 5–9, the fluoride anions are attracted to the positively charged surface of BCM2. Hence, the adsorption capacity is favored by the

electrostatic attraction between the fluoride in the solution and the BCM2 surface. The reduction in the adsorbing capacity by increasing the pH can be caused by a decrease in the surface charge of BCM2 (see Fig. 6). The surface charge and adsorption capacity of BCM2 were reduced around 9.2 and 6.3 times, respectively, by incrementing the pH from 5 to 9, confirming that the electrostatic interactions play a significant role in the BCM2 capacity for adsorbing fluoride.

3.8 Dependence of the BCM2 adsorption capacity upon temperature

Figure 10 shows the temperature effect on the BCM2 capacity for adsorbing fluoride adsorption and was analyzed by assessing the fluoride isotherms in water solution at temperatures of 35, 25 and $15\text{ }^\circ\text{C}$ and $\text{pH} = 7$. As pictured in Fig. 10, the adsorption capacity is enhanced by incrementing the temperature from 15 to $35\text{ }^\circ\text{C}$, revealing that the fluoride adsorption on BCM2 is endothermic. For a fluoride concentration of 20 mg g^{-1} , the adsorbing capacity augmented 1.5-fold while the temperature rose from 15 to $35\text{ }^\circ\text{C}$. However, the most significant increment occurred by rising from 15 to $25\text{ }^\circ\text{C}$, while the adsorption capacity difference between 25 and $35\text{ }^\circ\text{C}$ is slight.

The subsequent relationship was employed to evaluate the isosteric adsorption heat:

$$(\Delta H_{\text{ads}})_q = \frac{R \ln \frac{C_2}{C_1}}{\frac{1}{T_2} - \frac{1}{T_1}} \quad (12)$$

where C_1 and C_2 are the equilibrium concentration of fluoride at the same equilibrium mass adsorbed and

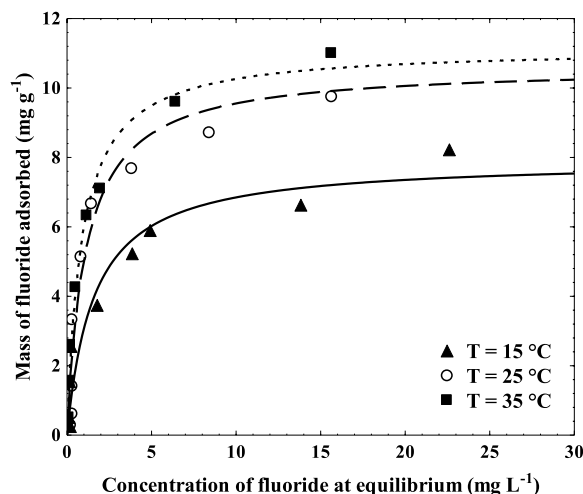
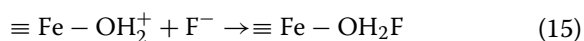


Fig. 10 Effect of temperature upon the capacity of BCM2 for adsorbing fluoride from aqueous solution at $\text{pH} = 7$. The lines represent the Langmuir isotherm predictions

at T_1 and T_2 , respectively, mg L^{-1} ; $(\Delta H_{\text{ads}})_q$ is the isosteric adsorption heat, J mol^{-1} ; R is the gas constant, $8.314 \text{ J mol}^{-1} \text{ K}^{-1}$; T_1 and T_2 are the temperatures at two different conditions, K . At $q=5 \text{ mg g}^{-1}$, the value of $(\Delta H_{\text{ads}})_q$ was about 26 kJ mol^{-1} , confirming that the process is endothermic so that the adsorption mechanisms are physical since the $(\Delta H_{\text{ads}})_q$ was less than 40 kJ mol^{-1} [37].

3.9 Adsorption mechanism of fluoride on BCM2

As indicated earlier, fluoride adsorption occurred predominantly on the basic sites. The primary adsorption mechanism was the electrostatic attraction between the protonated basic sites and F^- anions in water solution, and the following reactions illustrate these interactions:



Medellin-Castillo et al. [34] suggested the first two reactions for the fluoride adsorption on BC. In the modification, the adsorption capacity Q_{15} of BCM2 was promoted 2.6 (9.5/3.6) times compared to that of BC, while the concentration of basic sites in BCM2 was enhanced 2.6 (5.40/2.11) fold due to affixing the Fe hydroxyls. Furthermore, the adsorption capacity of BCM2 diminished by increasing the pH because the positive surface charge of BCM2 was lowered due to the lessening of basic sites concentration. The above results corroborate that the

adsorption of fluoride was predominantly occurring on basic sites.

3.10 Comparing the capacities of diverse materials for adsorbing fluoride

In Table 4, the BCM2 adsorption capacity towards F^- is compared to those of some plain and modified conventional and novel adsorbents. The adsorption capacities of various activated carbons modified by impregnation with Al(III) and Ce(III) varied between 0.9 and 4.6 mg g^{-1} [16, 38]. Table 4 shows that the adsorption of conventional materials such as $\gamma\text{-Al}_2\text{O}_3$, hydroxyapatite nanoparticles and Al_2O_3 nanoparticles ranged from 3 to 9.2 mg g^{-1} [39–41]. Various novel materials of mixed rare earth elements modified chitosan [42], nano-hydroxyapatite-stilbite composite [43], graphene oxide/alumina nanocomposite [39] and cellulose impregnated with Lanthanum [13] presented adsorption capacities between 4.7 and 9.7 mg g^{-1} , respectively.

The adsorption capacity of the commercial BC used in this study is 4.2 mg g^{-1} at pH 7 and $25 \text{ }^\circ\text{C}$, which is within the range of values reported in the technical literature. For example, the adsorption capacity of BCs commercially available in Mexico [21], Brazil [44] and Ethiopia [43] are 5.4 , 4.8 and 2.7 mg g^{-1} , respectively. The adsorption capacities of BCMs doped with metals and acid treated were higher than that of BC and varied from 6.8 and 14.4 mg g^{-1} . Thus, the modification enhanced the adsorption capacity of BC. The BCM2 presented the highest adsorption capacity towards fluoride, slightly higher than those of Ce(IV)-doped BC and the polymeric resin Amberlite-410. One advantage of BCM2

Table 4 Comparison of adsorption capacities of various materials towards fluoride in aqueous solution

Adsorbent	Maximum adsorption capacity (mg g^{-1})	Experimental conditions	Reference
Al impregnated activated carbon	0.90	pH 7, $25 \text{ }^\circ\text{C}$	[16]
$\gamma\text{-Al}_2\text{O}_3$	3.04	pH 6, $25 \text{ }^\circ\text{C}$	[7, 39]
Mixed rare earths modified chitosan	3.72	$30 \text{ }^\circ\text{C}$	[42]
Nano-hydroxyapatite-stilbite composite	4.02	$23 \text{ }^\circ\text{C}$	[43]
Commercial BC	4.07	pH 7, $25 \text{ }^\circ\text{C}$	This work
Ce(III) impregnated activated carbon	4.1–4.6	pH 6, $25 \text{ }^\circ\text{C}$	[38]
Graphene Oxide-Alumina Nanocomposite	4.68	pH 6, $25 \text{ }^\circ\text{C}$	[39]
Hydroxiapatite nanoparticle	7.0	pH 3, $25 \text{ }^\circ\text{C}$	[40]
Al-doped BC	6.8	pH 7.4, $25 \text{ }^\circ\text{C}$	[23]
BC treated with 1.0 M HNO_3 solution	7.74	pH 5, $25 \text{ }^\circ\text{C}$	[22]
Al_2O_3 nanoparticles	9.16	pH 5.4, $25 \text{ }^\circ\text{C}$	[41]
Cellulose impregnated with Lanthanum	9.7	pH 4–6, $25 \text{ }^\circ\text{C}$	[13]
Ce(IV)-doped BC	13.6	pH 7, $30 \text{ }^\circ\text{C}$	[24]
Ion exchange resin Amberlite IRA-410	13.8	pH 7, $25 \text{ }^\circ\text{C}$	[16]
BC modified with iron sulfate, BCM2	14.4	pH 5, $25 \text{ }^\circ\text{C}$	This work

over Amberlite-410 is that BCM2 is prepared by modifying charring animal bones, which is a waste. Besides, the BCM2 is cheaper to prepare than the Ce(IV)-doped BC because the Ce(IV) chemical reagent is more expensive than the Fe(II)/Fe(III) chemical reagents used in the BCM2 synthesis.

4 Conclusions

The BC and BCMs were mesoporous materials, as confirmed by their textural properties, and the modification decreased the surface area of the BCMs compared to that of BC. The surface charge distribution of BC and BCM2 demonstrated that the surface nature of both materials was basic. The determination of active sites indicated that the concentration of basic sites of BCM2 was 3.4-fold larger than that of acid sites, corroborating that the surface of BCM2 has a basic character. Furthermore, the basic sites concentration of BCM2 was 2.6 times greater than that of BC.

The SEM and TEM analysis showed that BCM2 had a similar morphology to BC; however, the modification reduced the surface irregularities and made a more homogeneous surface. The EDS microanalysis technique corroborated the presence of C, Ca, Fe, Na, O, P and S in BCM2. The XRD analysis verified the existence of hydroxyapatite in BC and BCM2.

The BCMs capacity for adsorbing fluoride was dependent upon the experimental conditions employed for modifying the BC, and the BCM2 presented the highest adsorption capacity, and its modifying conditions was considered optimal. The basic sites of BC and BCMs played a vital function in the adsorption capacity because the adsorption capacity increased almost linearly with the concentration of basic sites. The pH considerably affected the adsorption capacity of BCM2, which was enhanced approximately sixfold by diminishing the pH from 9 to 5. This shift was caused by the electrostatic attraction between the surface of the BCM2 and the fluoride in the water solution. The adsorbing capacity diminished 1.5 times by reducing the temperature from 35 to 15 °C, so the fluoride adsorption on BCM2 was endothermic.

Authors' contributions

DEVm carried out data curation, methodology, investigation, writing-original draft preparation and visualization. RLR performed funding acquisition, investigation, project administration, supervision, methodology, writing, reviewing and editing. CVM carried out data curation, investigation and visualization. EMM performed conceptualization, supervision, methodology, writing and visualization. NAMC accomplished conceptualization, supervision, methodology, writing, reviewing and editing. BAJL carried out data curation, investigation, writing and visualization. DHCA engaged in data curation, supervision, reviewing and editing. All authors read and approved the final manuscript.

Funding

DEVm thanks National Council for Science and Technology (CONACyT) for the Postdoctoral fellowship (CVU No. 554081) granted to pursue research in

Chemical Engineering at UASLP. Additionally, EMM is grateful to CONACyT for the Cathedra's program, project No. 864.

Availability of data and materials

Datasets used during the current study are available from the corresponding author on reasonable request.

Declarations

Competing interests

The authors declare they have no competing interests.

Received: 1 August 2022 Accepted: 14 January 2023

Published online: 08 February 2023

References

- Jensen O, Wu H. Urban water security indicators: development and pilot. *Environ Sci Policy*. 2018;83:33–45.
- WHO, UNICEF. Progress on Household Drinking Water, Sanitation and Hygiene 2000–2020: Five Years into the SDGs. Geneva and New York: World Health Organization and United Nations Children's Fund; 2021.
- WHO. Guidelines for Drinking-Water Quality: First Addendum to the Fourth Edition. Geneva: World Health Organization; 2017.
- Ghosh A, Mukherjee K, Ghosh SK, Saha B. Sources and toxicity of fluoride in the environment. *Res Chem Intermediat*. 2013;39:2881–915.
- Mohapatra M, Anand S, Mishra BK, Giles DE, Singh P. Review of fluoride removal from drinking water. *J Environ Manage*. 2009;91:67–77.
- Alkurdj SSA, Al-Juboori RA, Bundschuh J, Hamawand I. Bone char as a green sorbent for removing health threatening fluoride from drinking water. *Review Environ Int*. 2019;127:704–19.
- Das DP, Das J, Parida K. Physicochemical characterization and adsorption behavior of calcined Zn/Al hydroxalcalite-like compound (HTIC) towards removal of fluoride from aqueous solution. *J Colloid Interf Sci*. 2003;261:213–20.
- Jadhao VK, Kodape S, Junghare K. Optimization of electrocoagulation process for fluoride removal: a blending approach using gypsum plaster rich wastewater. *Sustain Environ Res*. 2019;29:1–9.
- Mbabaye GK, Mtalo F, Minja RJA, Legonda I. Standardizing defluoridation of community waters using bone char. *J Water Suppl Res T*. 2017;66:131–9.
- Leyva-Ramos R, Medellín-Castillo NA, Jacobo-Azuara A, Mendoza-Barron J, Landin-Rodríguez LE, Martínez-Rosales JM, et al. Fluoride removal from water solution by adsorption on activated alumina prepared from pseudo-boehmite. *J Environ Eng Manag*. 2008;18:301–9.
- Meenakshi S, Viswanathan N. Identification of selective ion-exchange resin for fluoride sorption. *J Colloid Interf Sci*. 2007;308:438–50.
- Ramirez-Llamas LA, Leyva-Ramos R, Jacobo-Azuara A, Martínez-Rosales JM, Isaacs-Paez ED. Adsorption of fluoride from aqueous solution on calcined and uncalcined layered double hydroxide. *Adsorp Sci Technol*. 2015;33:393–410.
- Nagaraj A, Sadasivuni KK, Rajan M. Investigation of lanthanum impregnated cellulose, derived from biomass, as an adsorbent for the removal of fluoride from drinking water. *Carbohydr Polym*. 2017;176:402–10.
- Tripathy SS, Raichur AM. Abatement of fluoride from water using manganese dioxide-coated activated alumina. *J Hazard Mater*. 2008;153:1043–51.
- Ganvir V, Das K. Removal of fluoride from drinking water using aluminum hydroxide coated rice husk ash. *J Hazard Mater*. 2011;185:1287–94.
- Leyva-Ramos R, Ovalle-Turrubiarres J, Sanchez-Castillo MA. Adsorption of fluoride from aqueous solution on aluminum-impregnated carbon. *Carbon*. 1999;37:609–17.
- Fang L, Ghimire KN, Kuriyama M, Inoue K, Makino K. Removal of fluoride using some lanthanum (III)-loaded adsorbents with different functional groups and polymer matrices. *J Chem Technol Biot*. 2003;78:1038–47.
- Luo F, Inoue K. The removal of fluoride ion by using metal (III)-loaded amberlite resins. *Solvent Extr Ion Exc*. 2004;22:305–22.
- Chen YN, Chai LY, Shu YD. Study of arsenic (V) adsorption on bone char from aqueous solution. *J Hazard Mater*. 2008;160:168–72.

20. Leyva-Ramos R, Medellín-Castillo NA, Flores-Cano JV. Bone char: Adsorbent manufactured from animal bones waste. Adsorption of fluoride from aqueous solution. *Bol Grupo Espanol Carbon*. 2015;36:2–5.
21. Medellín-Castillo NA, Leyva-Ramos R, Ocampo-Perez R, Garcia-De la Cruz RF, Aragon-Pina A, Martínez-Rosales JM, et al. Adsorption of fluoride from water solution on bonechar. *Ind Eng Chem Res*. 2007;46:9205–12.
22. Medellín-Castillo NA, Padilla-Ortega E, Tovar-García LD, Leyva-Ramos R, Ocampo-Perez R, Carrasco-Marin F, et al. Removal of fluoride from aqueous solution using acid and thermally treated bone char. *Adsorption*. 2016;22:951–61.
23. Nigri EM, Cechinel MAP, Mayer DA, Mazur LP, Loureiro JM, Rocha SDF, et al. Cow bones char as a green sorbent for fluorides removal from aqueous solutions: batch and fixed-bed studies. *Environ Sci Pollut R*. 2017;24:2364–80.
24. Zuniga-Muro NM, Bonilla-Petriciolet A, Mendoza-Castillo DI, Reynel-Avila HE, Tapia-Picazo JC. Fluoride adsorption properties of cerium-containing bone char. *J Fluorine Chem*. 2017;197:63–73.
25. Asfaram A, Ghaedi M, Hajati S, Goudarzi A. Synthesis of magnetic γ -Fe₂O₃-based nanomaterial for ultrasonic assisted dyes adsorption: Modeling and optimization. *Ultrason Sonochem*. 2016;32:418–31.
26. Boehm HP. Some aspects of the surface chemistry of carbon blacks and other carbons. *Carbon*. 1994;32:759–69.
27. Flores-Cano JV, Leyva-Ramos R, Mendoza-Barron J, Guerrero-Coronado RM, Aragon-Pina A, Labrada-Delgado GJ. Sorption mechanism of Cd(II) from water solution onto chicken eggshell. *Appl Surf Sci*. 2013;276:682–90.
28. Brunauer S, Emmett PH, Teller E. Adsorption of gases in multimolecular layers. *J Am Chem Soc*. 1938;60:309–19.
29. Ko DCK, Porter JF, McKay G. Mass transport model for the fixed bed sorption of metal ions on bone char. *Ind Eng Chem Res*. 2003;42:3458–69.
30. Rouquerol J, Rouquerol F, Llewellyn P, Maurin G, Sing KSW. Adsorption by powders and porous solids. Principles, methodology and applications. 2nd ed. Amsterdam: Elsevier; 2014.
31. Lowell S, Shields JE, Thomas MA, Thommes M. Characterization of porous solids and powders: surface area, pore size and density. Berlin: Springer; 2006.
32. Mansour SF, El-dek SI, Ahmed MA, Abd-Elwahab SM, Ahmed MK. Effect of preparation conditions on the nanostructure of hydroxyapatite and brushite phases. *Appl Nanosci*. 2018;6:991–1000.
33. Villela-Martínez DE, Leyva-Ramos R, Aragon-Pina A, Navarro-Tovar R. Arsenic elimination from water solutions by adsorption on bone char. Effect of operating conditions and removal from actual drinking water. *Water Air Soil Poll*. 2020;231:201.
34. Medellín-Castillo NA, Leyva-Ramos R, Padilla-Ortega E, Ocampo-Perez R, Flores-Cano, JV, Berber-Mendoza, MS. Adsorption capacity of bone char for removing fluoride from water solution. Role of hydroxyapatite content, adsorption mechanism and competing anions. *J Ind Eng Chem*. 2014;20:4014–21.
35. Villela-Martínez, DE. Eliminación de compuestos tóxicos en solución acuosa por medio de adsorción sobre carbonizado de hueso sin modificar y modificado y geles de carbono [Ph.D. Dissertation]. San Luis Potosí: Autonomous University of San Luis Potosí; 2020 [in Spanish].
36. Villela-Martínez DE, Leyva-Ramos R, Mendoza-Barron J. Removal of As(V) from water by adsorption on iron nanoparticles supported on bone char. In: 6th International Congress on Arsenic in the Environment. Stockholm; 2016 Jun 19–23.
37. Leyva-Ramos R. Importance and applications of liquid phase adsorption. In: Moreno-Pirajan JC, editor. Porous solids. preparation, characterization and applications. Bogotá: Ediciones Uniandes; 2007. p. 155–211 [in Spanish].
38. Raychoudhury T, Boindala SP, Kalidindi S. Performance evaluation of metal impregnated activated carbon composite for removal of fluoride under varying solution chemistry. *Water Sci Tech-W Sup*. 2017; 17:1377–85.
39. Xu NC, Li SX, Li W, Liu Z. Removal of fluoride by graphene oxide/alumina nanocomposite: Adsorbent preparation, characterization, adsorption performance and mechanisms. *ChemistrySelect*. 2020; 5:1818–28.
40. Maity JP, Hsu CM, Lin TJ, Lee WC, Bhattacharya P, Bundschuh J, et al. Removal of fluoride from water through bacterial-surfactin mediated novel hydroxyapatite nanoparticle and its efficiency assessment: Adsorption isotherm, adsorption kinetic and adsorption thermodynamics. *Environ Nanotechnol Monit Manag*. 2018;9:18–28.
41. Hafshejani LD, Tangsir S, Daneshvar E, Maljanen M, Lahde A, Jokiniemi J, et al. Optimization of fluoride removal from aqueous solution by Al₂O₃ nanoparticles. *J Mol Liq*. 2017;238:254–62.
42. Liang P, Zhang Y, Wang DF, Xu Y, Luo L. Preparation of mixed rare earths modified chitosan for fluoride adsorption. *J Rare Earth*. 2013;31:817–22.
43. Sani T, Gomez-Hortiguera L, Perez-Pariente J, Chebude Y, Diaz I. Defluoridation performance of nano-hydroxyapatite/stilbite composite compared with bone char. *Sep Purif Technol*. 2016;157:241–8.
44. Nigri EM, Bhatnagar A, Rocha SDF. Thermal regeneration process of bone char used in the fluoride removal from aqueous solution. *J Clean Prod*. 2017;142:3558–70.

Publisher's Note

Springer Nature remains neutral with regard to jurisdictional claims in published maps and institutional affiliations.

Ready to submit your research? Choose BMC and benefit from:

- fast, convenient online submission
- thorough peer review by experienced researchers in your field
- rapid publication on acceptance
- support for research data, including large and complex data types
- gold Open Access which fosters wider collaboration and increased citations
- maximum visibility for your research: over 100M website views per year

At BMC, research is always in progress.

Learn more biomedcentral.com/submissions

